Published in final edited form as:
Opt Lett. 2012 November 1; 37(21): 4443–4445.

Imaging a full set of optical scattering properties of biological tissue by inverse spectroscopic optical coherence tomography

Ji Yi* and **Vadim Backman**
Department of Biomedical Engineering, Northwestern University, 2145 Sheridan Rd., Evanston 60208, USA

Abstract

We here develop a method to measure and image the full optical scattering properties by inverse spectroscopic optical coherence tomography (ISOCT). Tissue is modelled as a medium with continuous refractive index (RI) fluctuation and such a fluctuation is described by the RI correlation functions. Under the first-order Born approximation, the forward model is established for ISOCT. By measuring optical quantities of tissue including the scattering power (SP) of the OCT spectrum, the reflection albedo a defined as the ratio of scattering coefficient μ_s and backscattering coefficient μ_b, we are able to inversely deduce the RI correlation function and image the full set of optical scattering properties.

As an important approach to provide quantitative guidance for disease diagnosis or screening, measurement of tissue optical properties plays a key role in biophotonics research. Methods have been developed to measure optical properties in various ways. [1] Imaging techniques such as confocal reflectance microscopy [2], optical coherence tomography (OCT) [3] and quantitative phase imaging [4] are able to quantify spatially-resolved optical properties. However, the above-mentioned methods are insufficient to measure the full set of optical properties *in vivo* due to the backscattering detection scheme for noninvasive measurement, which only allows sampling over a small angular extent of the scattering field.

Here, we propose a novel methodology to measure and image the full set of optical properties using ISOCT. The forward model of ISOCT regards tissue as a medium with a continuously varying refractive index (RI). Since RI fluctuation in tissue is weak, the optical scattering properties can be derived under the first-order Born approximation. By the optical measurement of OCT, the RI spatial auto-correlation (RI correlation) function can be reversely deduced, and the entire optical scattering properties can be quantified. More importantly, the 3D imaging capability of OCT provides localized analysis which helps to directly visualize the optical properties.

The most comprehensive way to quantify a random continuous medium is to use the RI correlation function, which statistically characterizes the tissue structural distribution. We modelled the RI correlation function $C_n(\rho)$ by the Whittle-Matern (WM) functional family with three parameters: the deterministic factor D, the length scale of the correlation l_c and the scaling factor $\mathcal{N}_c$. The WM functional family covers essentially all the well-known functions. When $0 < D < 3$, the correlation function has the form of a power law for small ρ. When $3 < D < 4$, the correlation function forms a stretched exponential. When $D = 4$, the correlation function evolves into an exponential and approaches a Gaussian function when D

*Corresponding author: ji-yi@northwestern.edu.

goes infinity. l_c determines the upper length scale of the correlation function, beyond which the function rolls off to 0 quickly. $\mathcal{N}_c$ is a scaling factor representing the variance of the RI fluctuation.

$$C_n(\rho) = \mathcal{N}_c \cdot 2^{(5-D)/2} \left(\frac{\rho}{l_c}\right)^{(D-3)/2} K_{(D-3)/2}\left(\frac{\rho}{l_c}\right), \quad (1)$$

in which $K_\nu(\cdot)$ denotes the modified Bessel function of the second kind; and ρ is the spatial displacement.

Under the Born approximation, the differential scattering cross section per unit volume σ toward any direction can be analytically derived [5]

$$\sigma(\theta,\phi) = 2\mathcal{N}_c k^4 l_c^3 \Gamma(D/2) \frac{\left(1 - \sin^2(\theta)\cos^2(\phi)\right)}{\sqrt{\pi}\left(1+[2kl_c \sin(\theta/2)]^2\right)^{D/2}}, \quad (2)$$

where (θ, φ) denotes the scattering angle in a spherical coordinate system; k is the wave number; Γ denotes the gamma function; $(1 - \sin^2(\theta)\cos^2(\varphi))$ is the dipole factor with linearly polarized incidence on $\varphi = 0$ direction. We next defined the backscattering coefficient $\mu_b = 4\pi\sigma_b$, where σ_b is the backscattering cross section per unit volume when $\theta = \pi$,

$$\mu_b = \mathcal{N}_c 8\sqrt{\pi}\Gamma(D/2) k^4 l_c^3 \left(1+[2kl_c]^2\right)^{-D/2}. \quad (3)$$

Meanwhile, the scattering coefficient μ_s is by definition an integration of σ over all solid angles.

$$\mu_s = \mathcal{N}_c \frac{\sqrt{\pi}\Gamma(D/2-3)}{2k^2 l_c^3}\left[\left(1+\left(2k^2 l_c^2 (D/2-2)-1\right)\times 2k^2 l_c^2 (D/2-3)\right) - \left(1+2k^2 l_c^2 (D/2+1)+4k^4 l_c^4\left(4-3D/2+D^2/4\right)\right)\left(1+4k^2 l_c^2\right)^{1-D/2}\right]. \quad (4)$$

The reflection albedo a, defined here as the ratio of μ_b and μ_s, can then be written. Tissue usually satisfies $kl_c \gg 1$ [6] and $D > 2$ according to the following measurements. Under this condition, the expression of μ_b and μ_s can be simplified:

$$\begin{aligned} \mu_b &\approx 2^{3-D}\mathcal{N}_c\sqrt{\pi}\Gamma(D/2) l_c^{3-D} k^{4-D}, \quad (kl_c \gg 1) \\ \mu_s &\approx 2\mathcal{N}_c\sqrt{\pi}\Gamma(D/2-1) k^2 l_c, \quad (kl_c \gg 1 \& D>2) \end{aligned} \quad (5)$$

thus

$$\alpha \approx \Gamma(D/2)/\Gamma(D/2-1)(2kl_c)^{2-D}. \quad (6)$$

The phase function essentially has the shape of $\sigma(\theta, \varphi)$ only with normalization such that the integral over 4π is equal to unity. The anisotropic factor g is defined as the cosine average $\langle\cos(\theta)\rangle$ of the phase function, and is also a function of D, kl_c. [5] Since it has been derived previously, we will not repeat the equation here.

With the forward model, we attempt to solve the inverse problem for ISOCT. Since OCT has small NA, the squared intensity of OCT image I^2 is approximately proportional to the backscattering coefficient μ_b: [7,8]

$$I^2 = rI_0^2 \frac{\mu_b}{4\pi} L \exp(-2zn\mu_s), \quad (7)$$

where I_0 and L is the intensity and the temporal coherence length of the incidence, respectively; r is the reference reflectance coefficient; z is the depth and n is the mean RI of the tissue, taken as 1.38. As Fig. 1 shows, the maximum value of the I^2 measures μ_b; and the decay rate along depth measures μ_s based on Beer's law. Thus the reflection albedo a can be calculated. Further, the spectrum of μ_b can be analysed by the time-Fourier analysis in spectroscopic OCT [9], and fitted with a power law equation. The exponent (often called the scattering power, SP) is equal to $4 - D$ according to Equ. 5. With D and a, l_c can be deduced according to Equ. 6. Then the correlation functional form can be readily described by D and l_c. Therefore, the phase function in Equ. 2 and g can be quantified.

Experimentally, we used a conventional Fourier-domain OCT (FDOCT) system with a supercontinuum source providing an illumination bandwidth from 650-800nm. The axial resolution is ~1.5μm and the lateral resolution is ~10μm with an effective NA 0.04. The scanning range is 2×2 mm on the lateral plane(x×y) and the B-scan rate is 10 fps. The spectra were first normalized by the reference spectrum and the OCT A-lines were normalized by the intensity profile of the focused beam. The OCT spectra were extracted by a short frequency Fourier transform (SFFT) [9] with a spectral resolution of 15nm, relaxing the axial resolution to ~ 15μm.

To characterize our measurement, we first fabricated a solid Agarose gel phantom embedded with polystyrene microspheres. The averaged signal was obtained from 0.5×0.5mm^2 lateral area(in $x \times y$). The measurements of μ_b and μ_s were repeated at each wavelength during SFFT according to Equ. 7. As Fig. 2(a-b) shows, the experiment agrees with Mie theory (solid line)well and the error is within 0.05 and 0.22mm^{-1} for μ_b and μ_s respectively. Due to the finite spectral resolution in SFFT, the Mie spectra were smoothed with 15nm Gaussian windows. Further we used 0.87μm spheres phantom, varied the concentration and compared the averaged μ_b and μ_s over λ to the Mie prediction as in Fig. 2(c-d). μ_b fits with calculated value well over a range up to 1mm^{-1} and μ_s deviates from around 14mm^{-1}, above which multiple scattering starts contributing the signal.

Next we characterized the accuracy of measuring D from the SP. A phantom with different polystyrene microsphere composition was designed as Fig. 2(e) shows. The total spectrum smooths out the individual oscillatory spectra from each size of microsphere and exhibits a power law over the incident bandwidth. The averaged spectra were obtained over 0.05×1mm^2 area in $x \times y$. Figure 2(f) plots the comparison of D on our measurements with the calculated values, which is calculated by Mie theory also based on the SP according to Equ. 5. We used four sizes of spheres (diameter: 360, 300, 200 and 80 nm) to compose the phantoms and the volume ratio of spheres for individual D values are: 0/6/5/0 (D=4.12), 6/20/60/0 (D=3.42), 6/20/60/150 (D=2.26), 6/15/60/1000 (D=0.98), 0/0/0/1 (D=0.12). The accuracy of D measurement is ±0.20 with 90% confidence using a linear regression on the calibration curve. Combining the calibration of μb and μs, the accuracy of measuring g is within ±0.03.

With the system calibrated, we measured six rat organs *ex vivo* to demonstrate the feasibility of ISOCT. μ_s and μ_b were calculated from the entire bandwidth, so that l_c is calculated at the center wavelength 710nm in Equ. 6. With D and l_c, g were obtained as shown in Fig. 3(a) for four types of organs. The key parameters of the tested organs from one subject are summarized in Table 1. To justify our measurement, the g values of similar organs from the literature are listed as comparison. Each measurements are taken over 0.25×0.25mm^2 area in $x \times y$ and from the top 100μm tissue.

Figure 3(c-d) further demonstrate the capacity of imaging optical properties from an *ex vivo* rat buccal sample. The a and g values designate Hue, and the image intensity encodes Saturation and Value in the HSV space. Three prominent layers are keratinized epithelium(KE), stratified squamous epithelium(SE) and submucosa(SM), each of which is considered homogeneous and applicable to our method. The SE appears more translucent and its anisotropic factor is measured at 0.91 on average, compared the KE and SM at 0.85 and 0.81 on average, respectively. For a robust measurement, μ_s and μ_b were smoothed over lateral $0.05\times0.25 mm^2$ area in $x \times y$ for each layer and D is averaged over the entire layer. The attenuation along the depth is compensated by multiplying the A-line signal with an exponential function according to μ_s [10].

The key assumption of the model is the first-order Born approximation. Although discontinuity at boundaries exists in tissue, the small RI changes can still satisfy the approximation and thus the derivation from RI correlation function to the optical properties is still applicable. [6]

Acknowledgments

The authors acknowledge the financial support from NIH grant R01CA128641, R01EB003682 and NSF grant CBET-0937987.

References

1. Cheong W, Prahl S, Welch A. A review of the optical properties of biological tissues. Quantum Electronics, IEEE Journal of. 1990; 26:2166–2185.
2. Collier T, Follen M, Malpica A, Richards-Kortum R. Sources of scattering in cervical tissue: determination of the scattering coefficient by confocal microscopy. Appl. Opt. 2005; 44:2072–2081. [PubMed: 15835356]
3. Faber D, van der Meer F, Aalders M, van Leeuwen T. Quantitative measurement of attenuation coefficients of weakly scattering media using optical coherence tomography. Opt. Express. 2004; 12:4353–4365. [PubMed: 19483984]
4. Ding H, Wang Z, Liang X, Boppart SA, Tangella K, Popescu G. Measuring the scattering parameters of tissues from quantitative phase imaging of thin slices. Opt. Lett. 2011; 36:2281–2283. [PubMed: 21685993]
5. Rogers JD, İlker R. Çapoğlu, Backman V. Non-scalar elastic light scattering from continuous random media in the born approximation. Opt. Lett. 2009; 34:1891–1893. [PubMed: 19529738]
6. Çapoğlu, İlker R.; Rogers, JD.; Taflove, A.; Backman, V. Accuracy of the born approximation in calculating the scattering coefficient of biological continuous random media. Opt. Lett. 2009; 34:2679–2681. [PubMed: 19724530]
7. Kodach VM, Faber DJ, van Marle J, van Leeuwen TG, Kalkman J. Determination of the scattering anisotropy with optical coherence tomography. Opt. Express. 2011; 19:6131–6140. [PubMed: 21451637]
8. Bosschaart N, Faber DJ, van Leeuwen TG, Aalders MCG. Measurements of wavelength dependent scattering and backscattering coefficients by low-coherence spectroscopy. Journal of Biomedical Optics. 2011; 16:030503. [PubMed: 21456858]
9. Leitgeb R, Wojtkowski M, Kowalczyk A, Hitzenberger CK, Sticker M, Fercher AF. Spectral measurement of absorption by spectroscopic frequency-domain optical coherence tomography. Opt. Lett. 2000; 25:820–822. [PubMed: 18064195]
10. Xu C, Schmitt JM, Carlier SG, Virmani R. Characterization of atherosclerosis plaques by measuring both backscattering and attenuation coefficients in optical coherence tomography. Journal of Biomedical Optics. 2008; 13:034003. [PubMed: 18601548]

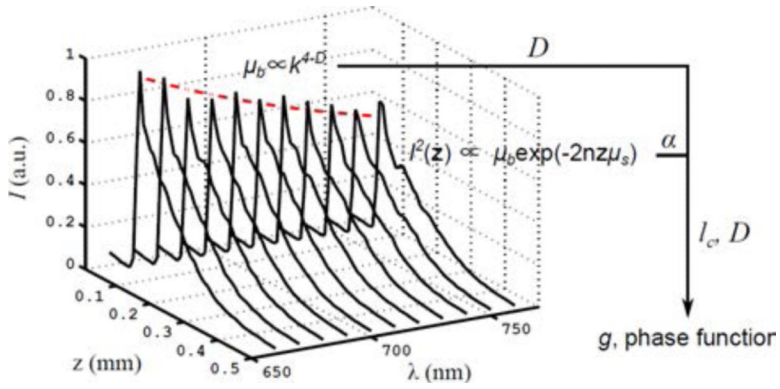

Fig. 1.

Schematic of the methodology. D is obtained from power law fitting to μ_b spectrum. l_c is deduced by D and α according to Equ.6.

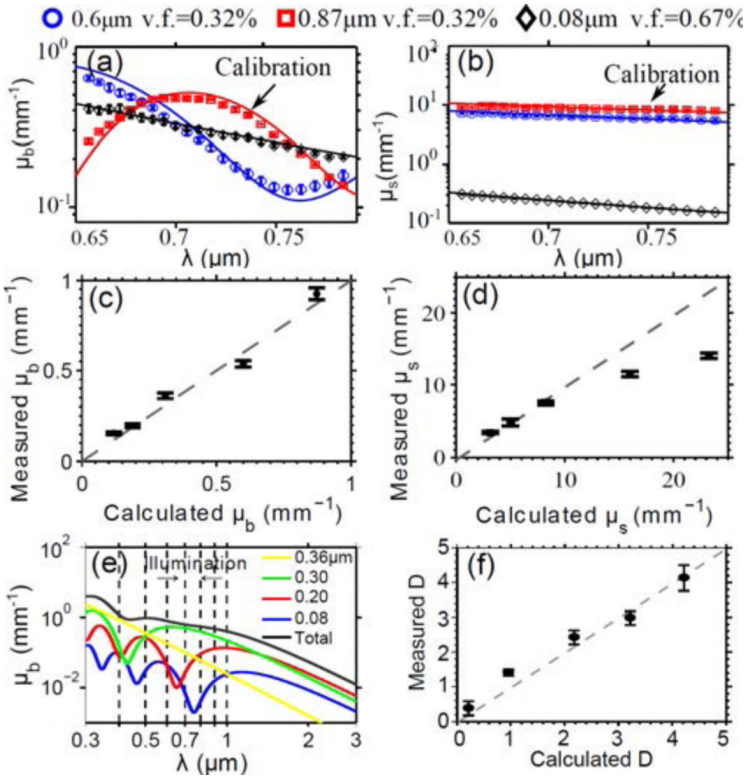

Fig. 2.

(a-b) μ_b and μ_s spectrum with the sphere diameters and volume fraction (v.f.). (c-d) Calibration of μ_b and μ_s in various concentrations of $0.87\mu m$ spheres. (e) D value phantom design with four types of spheres. The total spectrum is a power law within the illumination bandwidth. (f) Calibration of D. All the measurements were repeated three times. Error bar = *s.e.*

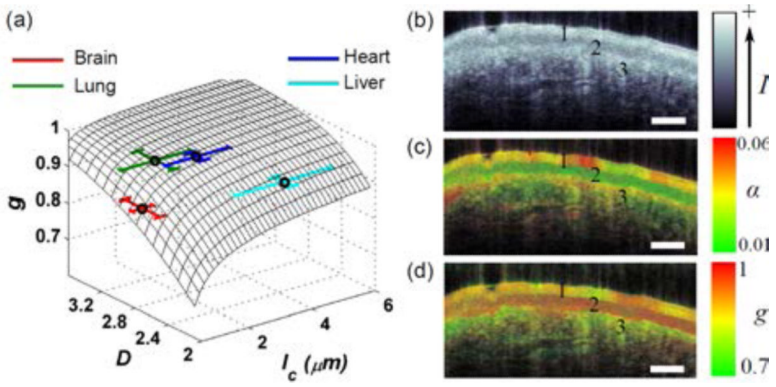

Fig. 3.

(a) Map of g dependence on D and l_c (b-d) Conventional OCT, a and g image from a rat buccal sample. (1)keratinized epithelium, (2)stratified squamous epithelium, (3)submucosa. Bar = 50μm

Table 1

Physical and optical properties ±*s.e.* of different rat organs (710nm)

	N	D	μ_s (mm^{-1})	μ_b (mm^{-1})	$l_c(\mu m)^a$	g^a	g from literature [1]
Brain	6	2.80 ±0.21	10.81 ±0.28	0.65 ±0.08	0.76 ±0.29	0.87 ±0.05	0.88 (633nm)
Liver	10	2.36 ±0.11	10.32 ±0.29	0.49 ±0.03	4.05 ±1.52	0.91 ±0.02	0.95 (630nm)
Lung(deflated)	9	3.02 ±0.20	11.42 ±0.29	0.11 ±0.02	1.75 ±1.04	0.95 ±0.04	0.95 (630nm)
Heart	9	2.84 ±0.08	13.26 ±0.37	0.27 ±0.06	2.59 ±0.96	0.96 ±0.02	0.973-0.983 (1060nm)
Intestine	7	3.06 ±0.15	7.80 ±0.23	0.05 ±0.01	2.78 ±1.42	0.97 ±0.03	
Spleen	7	2.98 ±0.19	13.28 ±0.30	0.26 ±0.09	1.71 ±1.13	0.95 ±0.03	

[a]Data were deduced and averaged from each measurements.